ADVANCED FUNCTIONAL MATERIALS
www.afm-journal.de

Prestrain-Free Dielectric Elastomers Based on Acrylic Thermoplastic Elastomer Gels: A Morphological and (Electro)Mechanical Property Study

*Pruthesh H. Vargantwar, A. Evren Özçam, Tushar K. Ghosh, and Richard J. Spontak**

Recent efforts have established that thermoplastic elastomer gels (TPEGs) composed of styrenic triblock copolymers swollen with a midblock-selective solvent exhibit remarkable electromechanical properties as high-performance dielectric elastomers. This class of electroactive polymers typically requires high electric fields for actuation, and a shortcoming that continues to thwart the widespread commercialization of such materials in general is the need to apply mechanical prestrain prior to electroactuation to decrease film thickness and, thus, the electric potential required to promote actuation. To alleviate this requirement, TPEGs consisting of acrylic triblock copolymers differing in molecular weight and composition, and swollen with a high dielectric, midblock-selective solvent are investigated. Synchrotron small-angle x-ray scattering is used to probe the nanoscale morphologies of the resultant materials, and analysis of quasi-static and cyclic tensile properties provides additional insight into both blend morphologies and electroactuation efficacy. Actuation strains measured in the absence of mechanical prestrain exceed 100% on an area basis, and electric fields capable of inducing actuation are as low as ~20 kV/mm. Failure occurs by either electromechanical instability or dielectric breakdown, depending on the copolymer and TPEG composition employed. The electromechanical properties of these acrylic-based TPEGs match or exceed those of skeletal muscle, in which case they constitute an attractive and unexplored alternative to existing dielectric elastomers.

1. Introduction

Triblock copolymers composed of glassy A endblocks and a rubbery B midblock are commonly classified as thermoplastic elastomers[1] (TPEs) and can be swollen with a low-volatility B-selective solvent to yield thermoplastic elastomer gels[2–4] (TPEGs), which continue to garner considerable scientific and technological interest as broadly functional materials. At copolymer concentrations below the critical micelle concentration (cmc), copolymer molecules remain in solution as unimers. As the copolymer concentration is increased above the cmc, however, micelles develop as the solvent-incompatible endblocks self-assemble to form a glassy core within a solvated shell of the solvent-compatible midblock.[5] Between the cmc and the critical gel concentration (cgc), so-called "flowered" micelles are sufficiently distant that the B midblocks form loops, wherein both ends of a copolymer molecule reside in the same micelle, or, to a lesser extent, thermodynamically unfavorable dangling ends, in which one endblock is located within a micelle and the other remains in the incompatible solvent matrix. At the cgc, the micelles are sufficiently close to permit the midblocks to connect (i.e., bridge) adjacent micelles and thus form a network physically stabilized by glassy cross-link sites.[2,6] The morphological features and mechanical properties of such gels depend sensitively on several material factors including copolymer composition, molecular weight and concentration, as well as solvent quality and free volume.[7,8] Most of the TPEGs studied thus far are based on styrenic copolymers, that is, copolymers with polystyrene endblocks and polydiene or polyolefin midblocks. Such TPEGs have gained tremendous attention as vibration dampeners,[9] pressure-sensitive adhesives,[10] microfluidic substrates,[11] and, most recently, dielectric elastomers.[12]

Another family of emerging TPEs relies on acrylic, rather than styrenic, endblocks to improve properties such as UV resistance and thermal stability over a broadened temperature range (due to a higher upper glass transition temperature, T_g).[13] The endblocks of such TPEs are frequently atactic poly(methyl methacrylate) (PMMA) with a T_g in excess of 120 °C, and the midblock is typically a low-T_g acrylate rubber such as poly(*n*-butyl acrylate) (PnBA), which possesses a T_g of about −50 °C at infinite molecular weight. Addition of a midblock-selective solvent to an acrylic TPE yields acrylic gels (ATPEGs) that are relatively new and unexplored. Shull and

P. H. Vargantwar, A. E. Özçam, Prof. R. J. Spontak
Department of Chemical and Biomolecular Engineering
North Carolina State University
Raleigh, NC 27695, USA
E-mail: Rich_Spontak@ncsu.edu
Prof. T. K. Ghosh
Department of Textile Engineering, Chemistry and Science
North Carolina State University
Raleigh, NC 27695, USA
Prof. R. J. Spontak
Department of Materials Science and Engineering
North Carolina State University
Raleigh, NC 27695, USA

DOI: 10.1002/adfm.201101985

co-workers[14,15] have pioneered this field by investigating the morphological characteristics and mechanical properties of such materials intended for use as adhesives. In their studies, they have employed high-vapor-pressure alcohols as the midblock-selective solvents, and the copolymer concentrations examined span the dilute to semi-dilute regimes. In this work, ATPEGs composed of two different PMMA-*b*-PnBA-*b*-PMMA (MBM) triblock copolymers differing in molecular weight and composition are examined in the presence of dioctyl phthalate (DOP), a midblock-selective solvent with a high normal boiling point (384 °C). Since most prior efforts have analyzed ATPEGs stabilized by spherical micelles, the present study is restricted to the concentrated copolymer regime so that structure-property relationships of ATPEGs possessing non-spherical morphologies can be elucidated. Moreover, these materials exhibit electroactuation properties that make them uniquely attractive as dielectric elastomers (DEs).

Electroactive polymers are macromolecules that are generally capable of changing their size and shape in response to the application of an external electric potential. As a growing class of electroactive polymers that shows tremendous promise for use in diverse technologies ranging from micro air vehicles and mini/microrobotics to flat panel speakers and responsive prosthetics, DEs, or electroelastomers, operate on the principle of electrostatic actuation in the presence of an applied electric field.[16–20] Actuation in this case results from the development of a compressive Maxwell stress, as described in more detail in the following section. Unlike their inorganic counterparts (e.g., shape-memory alloys,[21] carbon nanotubes[22] and piezoelectric ceramics[23]), DEs are relatively inexpensive, lightweight, mechanically robust, and scalable. They can afford exceptionally large area actuation strains (~300%), high energy densities (>8 MJ/m^3), high electromechanical coupling efficiencies (>90%), and low cycling hysteresis.[4] Our previous studies of DEs derived from styrenic copolymers selectively swollen with a largely aliphatic mineral oil have repeatedly demonstrated that TPEGs are ideally suited for this nontraditional application and, unlike conventional DEs produced from chemically crosslinked elastomers,[24] provide unprecedented versatility with regard to property design. Two drawbacks, however, continue to plague the commercialization of DEs: (i) a high electric field (typically ranging from ca. 20 to over 200 kV/mm) is required to induce electrical actuation, and (ii) mechanical prestrain is commonly needed to reduce specimen thickness and therefore lower the voltage required for actuation. The latter, in particular, necessitates a rigid support frame that is accompanied by added weight and space, and raises mechanical property concerns regarding long-time stress relaxation of the DE and premature failure of the DE upon cycling due to stress concentration along the frame. In the present study, we demonstrate that ATPEGs employed as nanostructured DEs can overcome both of the inherent shortcomings of contemporary DEs.

2. Electroactuation Background

The mechanism by which DEs undergo electrical actuation and stretch laterally derives from (i) the electrostatic force of attraction between two oppositely charged compliant electrodes on opposing sides of a DE film and (ii) the concurrent accumulation of repulsive like charges along both film surfaces. For an ideal DE, the magnitude of the resulting Maxwell stress (σ_M), portrayed in **Figure 1**, is given by[16]

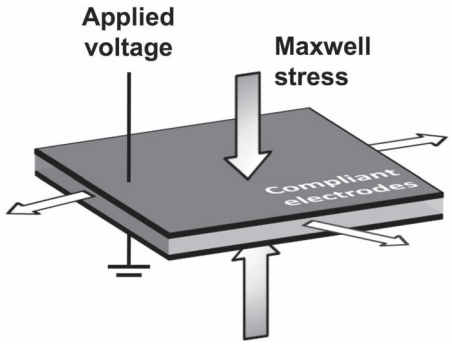

Figure 1. Schematic illustration of the general actuation mechanism exhibited by DEs. During actuation, electrostatic attraction of the oppositely charged compliant electrodes on each side of the DE film, coupled with repulsion of like charges along each electrode, generates a compressive stress referred to as the Maxwell stress (the magnitude of which is given by Equation 1 for an ideal DE) within the active area of the electrodes.

$$\sigma_M = \varepsilon_0 \varepsilon E^2 \quad (1)$$

where ε_0 and ε denote the permittivity of free space and the dielectric constant of the DE, respectively, and E represents the electric field arising from the voltage applied across the film thickness. The resulting actuation causes the film thickness to decrease while the active area corresponding to the compliant electrode expands in an isochoric process. The actuation strain (reported here on an area basis) is determined from the change in active area relative to the initial active area in the circular test configuration conventionally used to analyze the electroactuation of DEs. Alternatively, the transverse strain in the film thickness direction can be computed or measured directly.[19] Other important performance measures include the electromechanical coupling efficiency (K^2), which provides a measure of the conversion of electrical energy to mechanical work, and the energy density (F), which corresponds to the amount of electrical energy that is converted to mechanical work per volume of material per cycle.[16] In a recent study[25] of DEs composed of styrenic TPEGs, the ultimate electromechanical properties achieved during actuation — namely, the maximum actuation strain and the dielectric breakdown strength (i.e., the electric field at which failure occurs) — have been shown to depend on both the level of mechanical prestrain and the initial specimen thickness. If the copolymer used to prepare the TPEG is of sufficiently low molecular weight, maximum actuation strains of up to 20% and K^2 values of up to 30% can be realized[26] without mechanical prestrain prior to electroactuation. This response, although promising and superior to that of VHB (the benchmark DE composed of an acrylic elastomer and available as adhesive tape from 3M Co.), is insufficient for applications that, for example, emulate mammalian muscle, which exhibits higher performance metrics (cf. **Table 1**).[4,17,26]

Table 1. Comparison of electroactuation performance metrics for various systems with no mechanical prestrain.

Property	Mammalian skeletal muscle[17]		VHB4910 acrylic elastomer[26]	SEBS75 TPEGs[26]	ATPEGs
	Typical	Maximum	Maximum	Maximum[a)]	Maximum[a)]
Area actuation strain (%)	20	>40	8	3–19	12–10
Energy density (kJ/m^3)	8	40	6	1–26	18–49
Coupling efficiency (%)	—	40	14	6–29	21–77

[a)]Since the properties of TPEGs and ATPEGs are sensitive to copolymer concentration, a range is provided.

As anticipated, the electric fields and, hence, voltages needed to induce actuation in these tests are disappointingly higher than those required after mechanical prestrain.

3. Experimental Section

3.1. Materials

Two commercial MBM triblock copolymers were used in this study, and their designations, molecular characteristics and manufacturers are listed in **Table 2**. Reagent-grade DOP (98% purity) and toluene were purchased from Fisher Scientific and silver grease (i.e., silver particles suspended in a silicone matrix) was obtained from Chemtronics Circuit Works (Kennesaw, GA).

3.2. Sample Preparation

Each sample was prepared by dissolving predetermined quantities of copolymer and DOP, along with 1 wt% Irganox 1010 (as an antioxidant) relative to the copolymer concentration, in toluene and then casting the resultant solution in a Teflon tray and permitting the toluene to evaporate over 2 days. The ensuing film was annealed at 135 °C for 12 h under vacuum to remove residual toluene and subsequently melt-pressed at 135 °C to a uniform specimen thickness of 0.1–0.2 mm. The copolymer concentration in each ATPEG series ranged between 45 and 65 wt% in 5 wt% increments (this range corresponds to 20–30 vol% in the MBM104 series and 12–18 vol% in the MBM146 series). The ATPEGs produced in this fashion were designated as MBM*m*-*c*, where *m* denotes the number-average molecular weight of the copolymer (in kDa) and *c* indicates the copolymer concentration (in wt%). Comparisons made with other block copolymer systems follow the same naming convention. For example, SEBS75-45 identifies a TPEG composed of a poly[styrene-*b*-(ethylene-*co*-butylene)-*b*-styrene] (SEBS) triblock copolymer with a molecular weight of 75 kDa at a concentration of 45 wt% copolymer.

Table 2. Characteristics of the two MBM triblock copolymers used in this study.[a)]

Copolymer designation	Composition [wt% M]	Number-average molecular weight [kDa]	Polydispersity index	Manufacturer
MBM104	50.0	104	1.56	Arkema, Inc.
MBM146	31.3	146	1.04	Kuraray America

[a)]The molecular weight values listed here were measured by size exclusion chromatography (unlike those provided by the manufacturers in ref. 29).

3.3. Morphological Characteristics

Morphological features of ATPEGs from both copolymer series were deduced by small-angle X-ray scattering (SAXS) performed at 10 kV on beamline 7.3.3 of the Advanced Light Source at the Lawrence Berkeley National Laboratory. The beam size was 0.1 mm × 0.1 mm, and the sample-to-detector distance was held constant at 2.3 m. Two-dimensional scattering patterns were collected on a Pilatus 1M detector after an exposure time of 20 s and then azimuthally integrated and radially averaged to yield 1D profiles. In these profiles, scattered intensity was determined as a function of wave vector (q) given by $(4\pi/\lambda)\sin(\theta/2)$, where λ is the wavelength of the X-ray beam (0.1240 nm at 10 kV) and θ is the scattering angle, after correcting for dark background, specimen transmittance, pixel efficiency, and spatial heterogeneities in the beam. Specimens were heated to a target temperature at a rate of 10 °C/min and held at that temperature for 10 min to achieve thermal equilibration prior to data acquisition.

3.4. Mechanical and Thermal Properties

Each ATPEG examined here was subjected to uniaxial tensile testing on a computer-controlled MTS-30G load frame, and tests were performed to failure at a constant crosshead speed of 127 mm/min at ambient temperature. Properties such as the tensile modulus, strength at break and elongation at break were measured from the resulting nominal stress-strain plots. To discern the extent to which these ATPEGs exhibit hysteresis upon cyclic deformation, two types of strain cycling tests were conducted. In the first, each ATPEG was cycled (loading-unloading) 30× up to 100% strain. After 30 cycles, the nonrecoverable strain (set) was evaluated. The peak stress corresponding to 100% strain in each cycle was recorded to ascertain the extent of stress relaxation. In the second type of test, a specimen was strained to a selected stress value (σ_{max}) and released to a lower stress value (σ_{min}) chosen so that specimen slack was avoided. After completion of a cycle, σ_{max} was increased incrementally and the loading- unloading cycle was repeated with σ_{min} unchanged. This process was continued until σ_{max} approached the stress determined from the quasi-static uniaxial tensile tests performed to failure. To discern the effect of DOP on the thermal characteristics of the ATPEGs, differential scanning calorimetry (DSC) was performed on a TA Instruments Q2000 instrument operated from –125 to 170 °C at a constant heating/cooling rate of 10 °C/min under nitrogen. Glass transition temperatures were identified as points of inflection from second-heat thermograms.

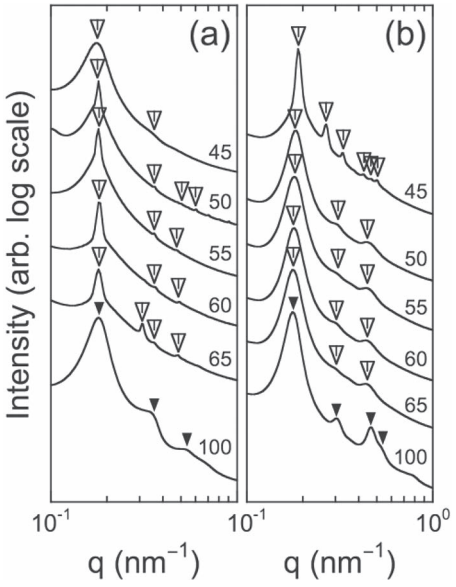

Figure 2. SAXS profiles acquired for the a) MBM104 and b) MBM146 ATPEG series at 135 °C (with the exception of the MBM104-45 formulation, which was measured at 90 °C to keep it below its order-disorder transition at ~120 °C, according to dynamic rheology). Scattering peaks are identified by open arrowheads, and copolymer concentrations (in wt%) are labeled.

3.5. Electromechanical Properties

The electroactuation behavior of each ATPEG was assessed at 0% mechanical prestrain unless otherwise noted. For this purpose, a circular active area was created on each test specimen by applying compliant electrodes (silver grease) on both sides of the specimen while the specimen was held in a circular, rigid test frame. Edge effects were precluded by ensuring that the active electrode area was small relative to the film area. The electrodes were connected to a Bertan 225-30R high-voltage power supply (Spellman High Voltage Electronics Corp., Hauppauge, NY), and actuation was induced by an automated voltage trigger. The voltage was ramped at 250 V/s until the specimen being tested underwent breakdown. As the voltage was ramped, in-plane expansion of the active area was digitally recorded, and the resulting footage was analyzed frame-by-frame with the MATROX Inspector 4.0 software package to determine the corresponding actuation strain. Dielectric constants of all the ATPEGs were measured in film form with a dielectric test fixture (Agilent 16451B) connected to an LCR meter (HP4284A) operated at 25 °C from 20 to 10^6 Hz.

4. Results and Discussion

4.1. Morphological characteristics

As shown in **Figure 2**, SAXS profiles acquired above the T_g of the M endblocks (106 °C in MBM104 and 121 °C in MBM146, according to the DSC results listed in **Table 3**) at 135 °C (except for MBM104-45) provide insight into the melt morphologies of the ATPEGs examined here, since they are processed at that temperature (see the Experimental Section). Here, only select scans relevant to the present work are shown, and a detailed account of additional results will be forthcoming. Peak ratios relative to the principal peak in the structure factor reveal the symmetry of the existing morphology. Peak ratios of 1:√2:√3:2:√5:√6, 1:√3:2:√7:√9 and 1:2:3:4 correspond to the classical morphologies: spheres on a body-centered cubic (bcc) lattice, cylinders on a hexagonal lattice and alternating lamellae, respectively. When the volume fractions of the endblocks are considered (20–30 vol% for MBM104 and 12–18 vol% M for MBM146),

Table 3. Thermal properties of the MBM104 and MBM146 ATPEGs according to DSC analysis.

ATPEG Series	Copolymer concentration [wt%]	Endblock T_g[a)] [°C]	Midblock T_g [°C]
MBM104	100	106.2	–46.5
	65	66.1	–72.7
	60	59.0	–73.9
	55	56.4	–74.5
	50	50.3	–76.3
	45	49.7	–77.7
MBM146	100	120.6	–41.7
	65	109.6	–72.6
	60	79.1	–76.9
	55	80.8	–75.4
	50	79.0	–76.5
	45	73.5	–77.5

[a)]Unlike the lower T_g, the upper T_g in many of the specimens tested was broad.

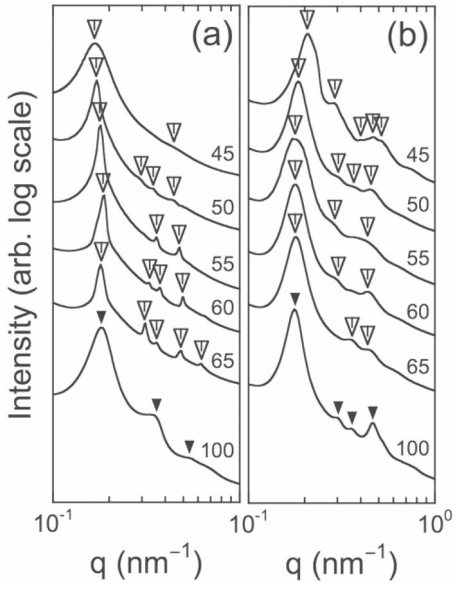

Figure 3. SAXS profiles acquired for the a) MBM104 and b) MBM146 ATPEG series at 35 °C (below T_g of the M endblocks). Scattering peaks are annotated in the same fashion described in the caption of Figure 2.

Table 4. Morphological details extracted from the SAXS patterns acquired from the MBM104 and MBM146 ATPEGs at 135 °C (in the melt) and 35 °C (with glassy endblocks).

Temperature [°C]	ATPEG Series	Copolymer concentration [wt%]	$2\pi/q^{*a)}$ [nm]	Peak ratios	Morphology
135	MBM104	100	34.9	1:1.97:2.96	Lamellar
		65	34.8	1:1.71:1.99:2.66	Cylindrical
		60	34.9	1:1.97:2.66	Cylindrical
		55	34.7	1:1.99:2.65	Cylindrical
		50	35.9	1:1.98:2.84:3.30	Cylindrical
		45	35.6	1:2.02	Uncertain
35	MBM104	100	34.9	1:1.97:2.96	Lamellar
		65	34.7	1:1.74:1.99:2.68:3.46	Cylindrical
		60	33.3	1:1.73:1.97:2.64	Cylindrical
		55	35.4	1:1.99:2.66	Cylindrical
		50	36.5	1:1.75:2.02:2.62	Cylindrical
		45	37.6	1:2.66	Uncertain
135	MBM146	100	35.7	1:1.73:2.65:3.02	Cylindrical
		65	35.7	1:1.71:2.46	Uncertain
		60	35.8	1:1.72:2.45	Uncertain
		55	34.6	1:1.70:2.43	Uncertain
		50	34.4	1:1.70:2.46	Uncertain
		45	33.3	1:1.42:1.75:2.25:2.44	Spherical
35	MBM146	100	35.2	1:1.71:2.01:2.65	Cylindrical
		65	35.0	1:2.02:2.45	Uncertain
		60	34.9	1:1.70:2.43	Uncertain
		55	34.9	1:1.63:2.43	Uncertain
		50	33.9	1:1.63:1.99:2.44	Uncertain
		45	30.4	1:1.41:1.96:2.25:2.49	Spherical

[a)] q^* denotes the wave vector of the principal scattering peak.

the morphologies that could be unambiguously assigned on the basis of peak ratios match well with the morphologies observed[7] in styrenic TPEGs. Since the MBM104 molecules are shorter than the MBM146 chains and are therefore able to self-organize more readily, long-range order is expected to be more fully developed in the ATPEGs generated from the MBM104 copolymer. On the basis of the peak ratios in the SAXS patterns displayed in Figure 2a and **Figure 3**a, the morphologies of the ATPEGs ranging in copolymer concentration from 50 to 65 wt% can be described as hexagonally-packed cylinders. Since higher-order peaks are not evident in the MBM104-45 system, the corresponding morphology could not be assigned with confidence. At the opposite extreme, the neat (i.e., non-solvated) copolymer is found to possess the lamellar morphology, which is consistent with the composition of the copolymer (~48 vol% M).

In the case of the ATPEGs produced from the MBM146 copolymer (cf. Figure 2b), only the morphology of the MBM146-45 formulation is clearly classified (as bcc spheres) from SAXS. At concentrations ranging from 50 to 65 wt% copolymer, the SAXS patterns appear similar, in which case these ATPEGs most likely possess identical morphologies. Regrettably, the lack of peaks in these patterns do not permit unambiguous discrimination between bcc spheres and hexagonally-packed cylinders (see **Table 4**). Elucidating these morphologies by electron microscopy, as well as the existence of order-(dis) order transitions by rheology and SAXS, is the focus of ongoing research and will be reported in a future publication. The neat MBM146 copolymer possesses a cylindrical morphology, which is consistent with the copolymer composition (~29 vol% M). This assignment further indicates that the unclassified morphologies exist between bcc spheres and hexagonally-packed cylinders and may represent a coexisting, frustrated mixture of the two or a nonequilibrated intermediate morphology (e.g., undulating cylinders), especially since the peak in the vicinity of 0.45 nm^{-1} is clearly present in each of the patterns. These morphological differences within and between the two ATPEG series can be reasonably expected to affect the corresponding (electro)mechanical properties, as interrogated in the following sections. Since all of the (electro)mechanical tests are conducted at ambient temperature, it is important to note that the morphologies identified in Figure 2 persist as the pure copolymers and their respective ATPEGs are cooled to ambient temperature, as evidenced by the SAXS patterns collected closer to

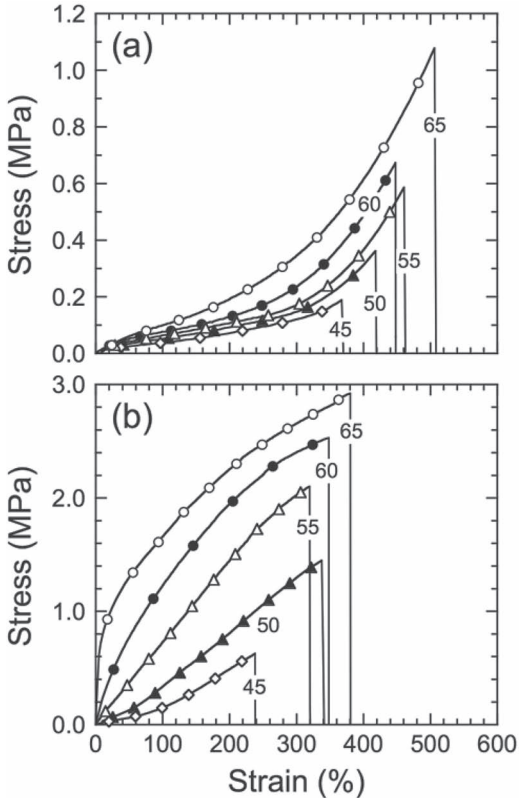

Figure 4. Nominal (engineering) stress displayed as a function of strain for the a) MBM146 and b) MBM104 ATPEGs at ambient temperature. Solid lines serve to connect the data (not all data points are shown), and copolymer concentrations (in wt%) are labeled.

ambient temperature (at 35 °C) and displayed in Figure 3. In this case, the endblocks are glassy, and shifts in the principal peak reflect dimensional changes that are introduced during vitrification. Comparison of the patterns in Figure 2 and 3 indicate that the morphologies classified at 135 °C are most likely retained upon vitrification of the M endblocks.

4.2. Mechanical properties

Representative nominal stress-strain curves are shown in **Figure 4** for ATPEGs in both copolymer series: (a) MBM146 and (b) MBM104. Several important features are evident in this figure. The first is that an increase in copolymer concentration is accompanied by increases in both the tensile modulus and the strength at failure in both series. These relationships are explicitly provided in **Figure 5**a and Figure 5b, respectively, and demonstrate that, in both cases, the mechanical properties of the ATPEGs derived from the MBM104 copolymer are more sensitive to copolymer concentration (due presumably to its higher M content) than are those containing the MBM146 copolymer. These property changes constitute a general consequence of increasing the concentration of the glassy M endblocks and are comparable to reports of styrenic copolymers in which the styrene content dominates the mechanical behavior.[27] The increase in modulus can be attributed to the effect of a reinforcing filler, viz., the M microdomains, whose population and size increase with increasing copolymer concentration. This explanation agrees favorably with the results of Seitz et al.,[28] who reported that the glassy domains in MBM-based ATPEGs influence the mechanical properties more than the network formed by bridged B midblocks. In general, the elongation at break likewise decreases (by comparable extents in both series) with decreasing copolymer concentration and can most likely be attributed to enhanced plasticization of the glassy M domains with DOP, as evidenced by lower glass transition temperatures at elevated DOP concentrations (from thermal calorimetry, cf. Table 3).

Comparison of the two copolymer series in Figure 4 also reveals a profound difference in stress evolution with strain. As above, the apparent stress–strain behavior can be interpreted in terms of the higher glassy content in ATPEGs consisting of the MBM104 copolymer. The steep rise in stress at low strain levels, the higher moduli and consequently higher stress values at break in the MBM104 series are due to the higher glassy content relative to the MBM146 series. Strain softening at intermediate strain levels (~200%) is a common characteristic of TPEGs, but is not observed in most of the MBM104 series in Figure 4b. One plausible explanation for this observation, as well as the higher moduli, is that cylinders, not spheres, exist in formulations with 50–65 wt% copolymer in the MBM104 series and offer greater resistance to deformation at low strains than do

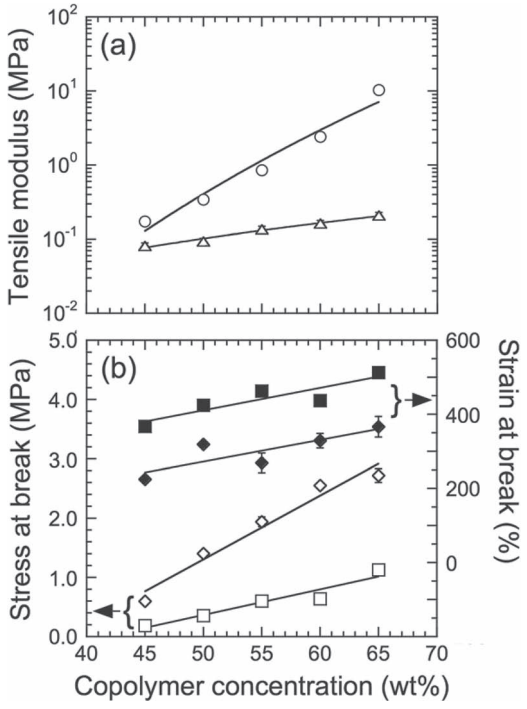

Figure 5. a) Tensile moduli measured at ambient temperature from uniaxial stress-strain curves and presented as a function of copolymer concentration for the MBM104 (○) and MBM146 (△) ATPEG series. b) Values of the stress (open symbols) and strain (filled symbols) evaluated at failure in both copolymer series: MBM104 (diamonds) and MBM146 (squares). Solid lines are straight lines through the data and serve as guides for the eye, and error bars correspond to the standard error in the data.

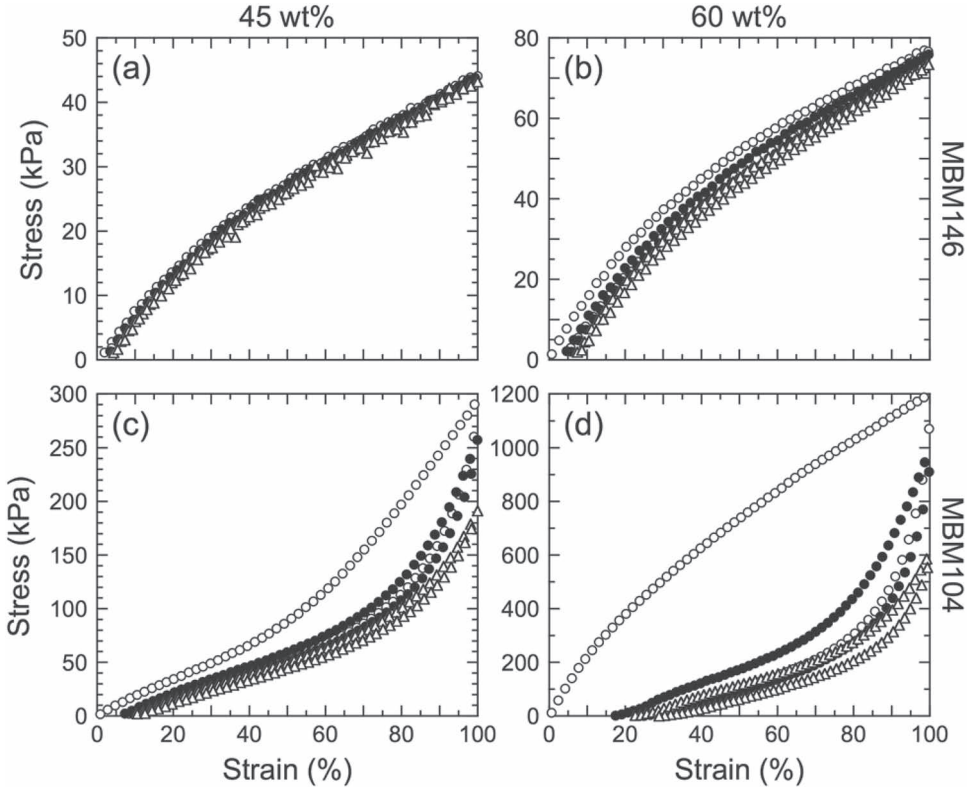

Figure 6. Cyclic tensile stress-strain curves obtained by loading and unloading a,b) MBM146 and c,d) MBM104 formulations with a,c) 45 and b,d) 60 wt% copolymer. For clarity, data collected from only the 1st (○), 2nd (•) and 30th (△) cycles are displayed. Hysteresis is evident from (i) the development of stress softening (the reduction in stress at the maximum applied strain), (ii) the area within loading-unloading loops and (iii) the non-recoverable strain, or set (the shift in curves along the strain axis upon cycling).

spheres. Laurer et al.[7] and Seitz et al.[28] independently report that cylindrical morphologies possess higher moduli than spherical ones in TPEGs and ATPEGs, respectively. At higher strains near failure, formulations in the MBM146 series in Figure 4a exhibit significant strain hardening as the midblocks approach full extension. In sharp contrast, ATPEGs derived from the MBM104 copolymer display evidence of strain softening at this limit in Figure 4b due to irreversible deformation and damage to the glassy M microdomains. Thus, the results presented in Figure 4 and 5 establish that the two ATPEG series considered in this study possess markedly different mechanical properties that relate to copolymer composition and morphology.

As DEs, these ATPEGs are required to withstand cyclic deformation. To determine their ability to do so, we have subjected them to multicycle uniaxial tensile deformation in two types of strain-cycling tests. In the first, specimens are cycled 30x between 0 and 100% strain, and the results are shown in **Figure 6** for two formulations (45 and 60 wt% copolymer) in the MBM104 and MBM146 series. In all cases examined, the nominal stress-strain response becomes independent of cycle number after about 25 cycles, which indicates that our choice of 30 cycles is sufficient to ascertain the cyclic deformation behavior of the present materials. To facilitate scrutinization of the data in Figure 6, only the 1st, 2nd and 30th loading-unloading loops are shown. In Figure 6a, the MBM146-45 formulation exhibits virtually indistinguishable loading-unloading loops with complete elastic recovery and little hysteresis (the level of unrecoverable strain is <5%) upon repeated tensile deformation, which is strikingly reminiscent of styrenic TPEGs discussed elsewhere.[29] Minimal stress softening is also apparent in multiple loading and unloading cycles over the strain range examined. Figure 6b shows, however, that the MBM146-60 formulation is more sensitive to cyclic loading and undergoes limited hysteresis, as evidenced by a small shift in the data at zero load to a higher unrecoverable strain (set) after just one cycle. After 30 cycles, however, the set remains at less than 10% strain. This specimen also undergoes stress softening that becomes detectable after the second cycle and that increases slightly with copolymer concentration. According to the results provided in **Figure 7**, the degree of stress softening, as determined from a reduction in the ratio of the peak stress measured at 100% strain (σ_n) during each cycle (n) to that measured after the first cycle (σ_1), remains negligibly small for all the ATPEGs produced from the MBM146 copolymer.

On the basis of their minimal hysteresis, set and stress softening due to cyclic deformation, it immediately follows that the MBM146-based ATPEGs appear suitable for use in continuous electroactuation applications. This is not the case, however, for formulations derived from the MBM104 copolymer. In Figure 6c and 6d, corresponding to the MBM104-45 and MBM104-60 systems, hysteretic losses due to cycling are pronounced and

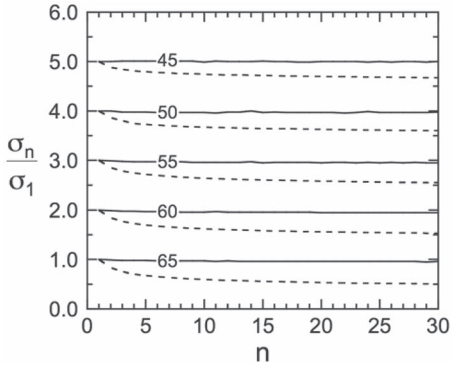

Figure 7. Stress softening evaluated from cyclic tensile stress-strain curves as the maximum stress of each cycle (σ_n) normalized by that of the first cycle (σ_1) and presented as a function of cycle number (n) for the MBM146 and MBM104 ATPEG series (solid and dashed lines, respectively). The curves are shifted vertically by one unit for clarity, and the copolymer concentrations (in wt%) are labeled.

become progressively worse as the copolymer concentration is increased. Stress softening is clearly discernible in all these ATPEGs and increases with increasing copolymer concentration (cf. Figure 7). For comparative purposes, the value of σ_{30}/σ_1 for the MBM104-65 formulation is 50%, in marked contrast to 96% for the MBM146-65 formulation under identical test conditions. Similarly, values of the set measured for both ATPEG series and included in **Figure 8** confirm that those generated from the MBM104 copolymer are considerably more sensitive to cycling than those derived from the MBM146 copolymer. In fact, set values determined for formulations with the MBM146 copolymer are typically less than or equal to 5%, whereas those for materials incorporating the MBM104 copolymer can exceed 35% after 30 cycles, suggesting that these systems may not be suited for use as actuators that could require millions of strain cycles during their active lifetime.

The mechanical properties of the ATPEGs under investigation here can be explained in light of their nanoscale morphologies. The prominent hysteresis loops, set and stress softening displayed by the MBM104-based ATPEGs upon cycling are largely attributed to the permanent deformation of glassy M

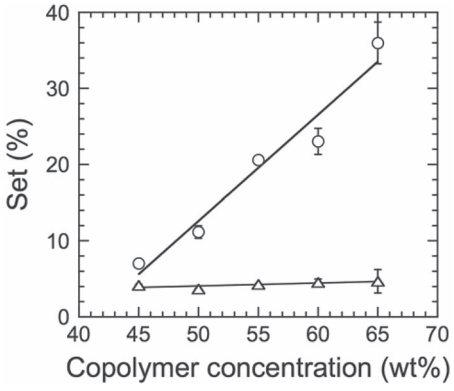

Figure 8. Dependence of non-recoverable strain (set) measured at the end of 30 loading-unloading cycles up to 100% strain on copolymer concentration for the MBM104 (○) and MBM146 (△) ATPEG series. Solid lines are linear fits to the data and serve as guides for the eye.

microdomains that, as cylinders, are discrete but potentially long and intertwined. In this case, the cyclic mechanical properties of network materials possessing anisotropic glassy microdomains are expected to display evidence of viscoelasticity, unlike analogous systems containing uniformly-dispersed, spherical M microdomains. Recall, for instance, that the MBM146-45 formulation possesses a spherical morphology according to SAXS (cf. Figure 2 and 3) and exhibits a nearly elastic response to cyclic deformation in Figure 6a. Comparable behavior is retained when the strain is doubled to 200%. These observations support the findings of Seitz et al.[28] and Mamodia,[30] who report that discretely distributed spheres suffer negligible deformation under uniaxial tension. Even under biaxial tension, the deformation of glassy spheres in a TPEG is minimal.[31] Another consideration here is the fraction of bridged midblocks, which dictates the connectivity of the network responsible for the mechanical integrity, as well as the recoverability, of a swollen triblock copolymer subjected to deformation. Matsen and Thompson[32] predict, on the basis of self-consistent field theory, that the fraction of bridged midblocks is the largest for the spherical morphology, in which case it immediately follows that the restorative capability of the midblock network decreases upon changing from a spherical to a cylindrical morphology.

Although the bridging fraction may differ considerably between spherical and cylindrical block copolymer morphologies, we do not believe that the bridge fraction changes appreciably during cyclic loading. The ATPEG series derived from the MBM104 copolymer, for instance, exhibits permanent deformation in all the formulations examined here. Except for MBM104-45 (whose morphology cannot be classified from SAXS), all other formulations possess hexagonally-packed cylinders, according to the SAXS patterns provided in Figures 2 and 3. In cyclic loading tests, the maximum damage to the material occurs during the first loading cycle, after which subsequent damage continues incrementally in subsequent cycles. Recovery achieved during the unloading cycles is due almost exclusively to the bridged midblocks. If M endblocks were to pull out from glassy micelles during deformation, the population of bridged midblocks would decrease and the unloading behavior, in turn, would most likely continue to evolve as the number of cycles increased. According to the data presented in Figure 6c and 6d (as well as additional data not shown for other formulations), the unloading curves appear similar in each cycle, strongly suggesting that the bridging fraction remains unchanged during tensile deformation under the test conditions employed here. Since the tests have been performed at ambient temperature (below T_g of the M blocks), we instead suspect that fracture or otherwise permanent deformation of the glassy cylindrical microdomains under loads exceeding their elastic limit is responsible for the results displayed in Figure 6–8. Results from the second cycling test (described in detail below) are consistent with this conclusion. In these tests, samples subjected to increasing stress after a single cycle to a predetermined stress show evidence of additional energy dissipation, softening and set consistent with increased deformation and/or fracture of the M cylinders. Similar behavior independently reported for ATPEGs on the basis of compression testing[15] and indentation techniques[28] has been ascribed to morphological differences deduced solely on the basis of composition.

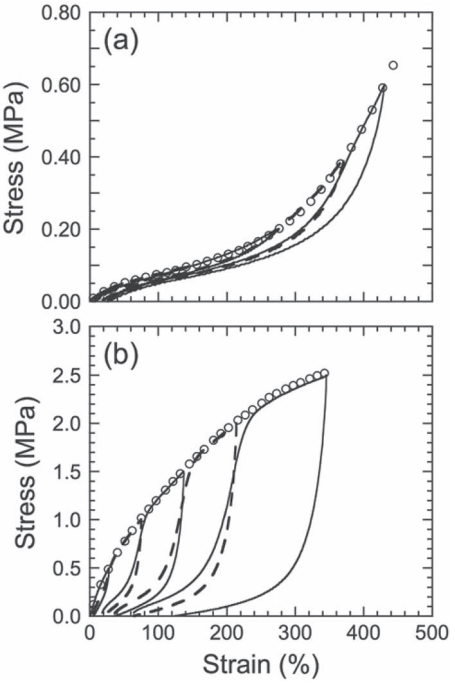

Figure 9. Cyclic tensile loading-unloading curves measured between stress points as the upper stress limit is progressively increased after completing 1 cycle for the a) MBM146 and b) MBM104 ATPEGs with 60 wt% copolymer. Subsequent cycles are differentiated by alternating solid and dotted lines. Corresponding data obtained from tensile tests conducted to failure (○, cf. Figure 4) are included.

Stress softening (cf. Figure 7) is a frequently encountered phenomenon widely referred to as the Mullins effect in filled rubbers[33] and crystallizing gums.[34] It has been interpreted[35] in terms of molecular-level processes such as molecular slippage, chain breakage and chain disentanglement and is manifested as a significant reduction in stress. Recently, this effect has been reported to occur in styrenic TPEs due to either strain-induced crystallization of the polyolefin midblocks (which depends on midblock composition and chain length) or microbuckling of glassy cylindrical or lamellar microdomains.[30,36] In the present study, midblock crystallization in the presence of DOP can be immediately ruled out, and so we only consider further the second possibility. To determine if the present ATPEGs display evidence of the Mullins effect, cyclic tensile tests have been performed between two stresses — a maximum (σ_{max}) and a minimum (σ_{min}) — with σ_{max} increased stepwise after completion of each cycle. Representative test results are provided in **Figure 9** for formulations containing 60 wt% copolymer in both series. Several features in this figure warrant discussion. The nominal stress-strain curves corresponding to loading and unloading in Figure 9a and 9b are strongly nonlinear and reminiscent of the data shown earlier in 6b and 6d, respectively. The hysteresis energy, as determined from the area between the loading and unloading curves in each cycle, increases noticeably as σ_{max} is increased in both systems and is attributed to an increase in the strain-induced damage to the glassy microdomains. When σ_{max} is subsequently increased after completing a loading–unloading cycle at a given stress, the stress–strain curve rapidly reaches the quasi-static tensile curve (cf. Figure 4) measured at the same composition (identified by open circles in Figure 9). According to Roos and Creton[9] and Drozdov,[37] this characteristic is a signature feature of the Mullins effect, thereby confirming our earlier conclusion.

On one hand, the Mullins effect is apparent at all compositions in the MBM104-based ATPEG series (data not shown), and it becomes more pronounced as the copolymer concentration is increased from 45 to 65 wt%. In the MBM146-45 formulation, on the other hand, evidence of the Mullins effect is completely absent, but becomes increasingly discernible with increasing polymer concentration. These observations are likewise consistent with the ATPEG morphologies assigned from SAXS, as well as the observations reported by Mamodia[30] for neat styrenic triblock copolymers. Glassy cylinders (in the MBM104 series) can undergo microbuckling and form a chevron-type pattern, which results in the Mullins effect. The increase in this effect with increasing copolymer concentration may reflect corresponding changes in the dimensions of the glassy cylinders, since resistance to fracture or permanent deformation depends on both cylinder size and modulus.[36] Although an experimentally corroborated correlation is not yet established between microdomain stiffness and the Mullins effect, variation in microdomain size with copolymer concentration could help to explain the property trends ascertained in the MBM104-based ATPEG series. In Figure 2a and 3a, for instance, the principal peak systematically broadens (which means that the cylindrical diameter correspondingly decreases) as the copolymer concentration is increased. This variation suggests that the Mullins effect, under comparable load cycling, becomes increasingly pronounced as the glassy cylinders become thinner. This observation is certainly amenable to further experimental verification and computer simulation. In the one formulation possessing an unequivocal spherical morphology (MBM146-45), no microbuckling of the glassy microdomains can occur and, hence, no Mullins effect is observed.

In the discussion above, we demonstrate that the Mullins effect is a consequence of the cylindrical microdomains in the ATPEGs produced from the MBM104 copolymer. Can this relationship help to identify the unclassified morphologies in the MBM104 and MBM146 series? Although electron microscopy, coupled with electron tomography[38] when necessary, is conventionally used to identify the morphology of microphase-separated block copolymer systems, the M and B blocks of the parent MBM copolymers are chemically similar and, as acrylics, are inherently resistant to most heavy-metal stains, thereby making selective staining to enhance phase contrast difficult, if at all possible. While such efforts remain underway, we turn our attention to an alternative and somewhat unconventional approach to morphological determination. If the SAXS patterns displayed in Figure 2 and 3 are considered in light of the mechanical property results provided in Figure 6–9, then additional insight into the morphologies of the unclassified formulations can be gleaned. First, recall that the undetermined MBM146 morphologies possess similar scattering patterns and are therefore considered to be the same. Second, these morphologies are likely to be dispersed since they reside between hexagonally-packed cylinders (MBM146-100) and bcc spheres (MBM146-45). Since spherical morphologies do not show

evidence of the Mullins effect,[30] the unclassified morphologies in the MBM146 series are most likely not spherical in nature. As they exhibit the Mullins effect to a relatively small degree, however, we suspect that the morphology is slightly anisotropic (to permit detectable strain-induced microdomain fracture or permanent deformation). Morphologies consistent with these requirements include short, stubby cylinders or, alternatively, ellipsoids that, because of their slight anisotropy, do not readily arrange on a lattice. Another possibility is a mixed morphology composed of spheres with a small fraction of cylinders that frustrate lattice packing and undergo strain-induced damage upon cycling. In the case of the undetermined MBM104-45 formulation, the Mullins effect is also clearly encountered. This feature, combined with the composition of this material (24 vol% M), strongly suggests that the morphology in this ATPEG is either cylindrical or a mixture of cylinders and spheres.

4.3. Electromechanical properties

Interest in selectively swollen triblock copolymer systems as DEs capable of being finely tuned in the manner by which they respond to an applied electric fields continues to grow, and this study represents the first attempt to employ ATPEGs for the purpose of being used as electromechanical actuators. While previous investigations of ATPEGs have utilized midblock-selective solvents with relatively high vapor pressures suitable for materials processing, use of high-boiling DOP as the midblock extender in the present study permits extended stabilization of the resulting materials for application purposes. Preferential compatibility between the copolymer midblock and DOP can be explained in terms of their solubility parameters (δ). The value of δ for the B midblock [9.1 $(cal/cm^3)^{1/2}$][39] is marginally closer to that of DOP [7.9 $(cal/cm^3)^{1/2}$][40] than is δ of the M endblock [9.3 $(cal/cm^3)^{1/2}$].[39] The difference in solvent quality relative to the copolymer blocks, coupled with the compositions and molecular weights of the two copolymers and the solvent concentrations examined, promotes micellization (spherical, cylindrical or an intermediate/mixture thereof) of M blocks embedded in a matrix of B blocks swollen with DOP. Due to the similarity in the chemical nature (and solubility parameters) of the blocks comprising the copolymers, however, the solubility of DOP in M cannot be ignored, in which case it is reasonable to expect that the micelles containing M cores are somewhat swollen by DOP. An undesirable ramification of DOP in the micellar cores is a reduction in the upper T_g due to plasticization of the endblocks, which serve as the physical cross-links responsible for network stabilization. Analysis of these depressed T_g values (listed in Table 3) by the Fox-Flory equation indicates that the DOP concentration within the micellar cores ranges from 3 to 17 wt%.

The mechanical properties reflecting the presence of a supramolecular micellar network and interrogated in the previous section confirm that at least some of the present ATPEGs are suitable candidates as DEs on the basis of their response to strain cycling. In this section, the dependence of electrical actuation without mechanical prestrain on copolymer concentration is ascertained for both series of ATPEGs and quantitatively compared with two other DEs previously measured under comparable test conditions:[26] (i) a SEBS75-45 TPEG composed of a styrenic triblock copolymer and reported to attain a maximum actuation strain of 7% with no mechanical prestrain, and (ii) the benchmark acrylic elastomer VHB4910, where the last 2 digits identify film thickness (in tenths of a millimeter). Recall that electroactuation depends on the development of a Maxwell stress that serves to compress the DE under examination. According to Eq. 1, σ_M in the case of an ideal DE is dependent on the dielectric constant of the DE (ε) and the applied electric field (E). Measured values of the real component of the complex dielectric constant (ε') are provided as a function of frequency for both copolymer series in **Figure 10** and reveal several important features. The first is that an increase in DOP concentration significantly increases ε' (in one case beyond 5.0), which is not surprising since the dielectric constant of pure DOP is 5.1. Whereas the VHB4910 acrylic elastomer exhibits a weak maximum in ε' at 100 Hz and decreases slightly, but monotonically, at higher frequencies, some of the current ATPEGs in the MBM146 series display a minimum in ε' at 100 Hz and then become almost independent of frequency at higher frequencies. In the MBM104 series, ε' decreases with increasing frequency, but not to the same extent as the acrylic elastomer. The dependence of ε' on copolymer concentration in both ATPEG series is provided at 10^3 and 10^6 Hz in **Figure 11** for completeness and confirms, as expected, that ε' tends to increase with decreasing copolymer (and increasing DOP) concentration in both series and at both frequencies.

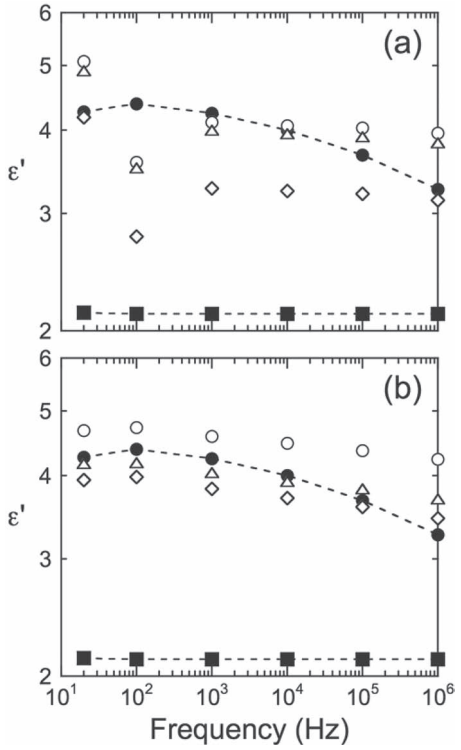

Figure 10. Frequency dependence of the real dielectric constant (ε') measured at three different copolymer concentrations (in wt%) in the a) MBM146 and b) MBM104 ATPEG series: 45 (○), 55 (△) and 65 (◇). Other ATPEGs not shown (for clarity) exhibit similar trends. Results from the VHB4910 acrylic elastomer (•) and SEBS75-45 TPEG (○) are included for comparison, and the dashed lines serve to connect the data.

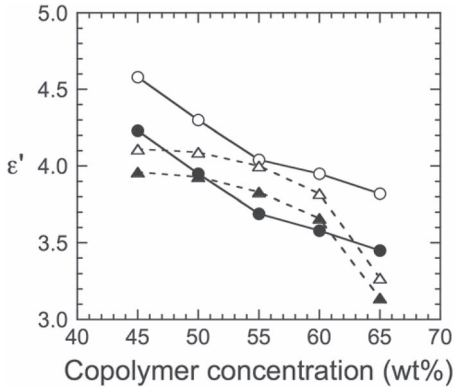

Figure 11. Dependence of ε' on copolymer concentration in the MBM104 (circles, solid lines) and MBM146 (triangles, dashed lines) ATPEG series evaluated at 10^3 (open symbols) and 10^6 (filled symbols) Hz. The solid and dashed lines serve to connect the data.

The results displayed in Figure 10 and 11 confirm that the dielectric properties of ATPEGs are composition-tunable and that these materials are electrically stable over a broad frequency range spanning over four decades. Such stability is critically important for high-frequency applications such as those requiring flapping or rippling motion (e.g., a micro air or underwater vehicle). Figure 10 also shows that measured values of ε' for the SEBS75-45 TPEG and the VHB4910 acrylic elastomer are lower (by up to 100% and 30%, respectively) compared to those of the present ATPEGs. This difference suggests that the ATPEGs under investigation are more prone to respond to an applied electric field. Once a test specimen is mounted on a circular support and compliant electrodes are painted on both sides of the specimen, an electric field is applied, and the ensuing actuation is directly evaluated from the lateral (in-plane) change in active area, as discerned from analysis of real-time video footage. Values of the maximum actuation strain, as well as the corresponding maximum transverse (thickness) strain, measured at failure for both ATPEG series at ambient temperature are displayed as a function of copolymer concentration in **Figure 12**. Included in this figure for comparison are results reported[26] for the SEBS75-45 TPEG and the VHB4910 acrylic elastomer without mechanical prestrain. At the lowest copolymer concentration investigated (45 wt%), the largest actuation strain occurs with the MBM146-45 formulation at ~115%, which is about 16x that of the SEBS75-45 TPEG and 14x that of the VHB4910 acrylic elastomer. Recall from Figure 2 and 3 that this material possesses a spherical morphology with no evidence of the Mullins effect during strain cycling. In both ATPEG series, an increase in copolymer concentration promotes reductions in the maximum actuation and transverse strain due to a decrease in high-ε DOP and an increase in modulus.

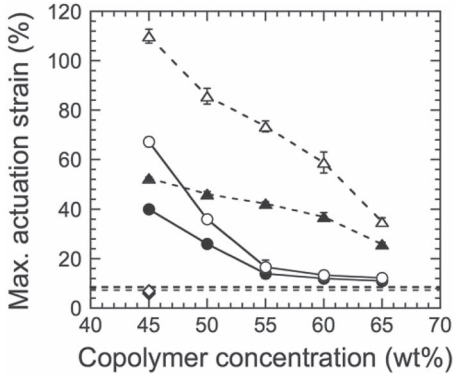

Figure 12. Maximum electroactuation-induced area (open symbols) and thickness (filled symbols) strains presented as functions of copolymer concentration for MBM104 (circles) and MBM146 (triangles) ATPEGs without mechanical prestrain conditions. Error bars correspond to the standard error in the data. The corresponding actuation metrics of the SEBS75-45 TPEG (diamonds) are included for comparison, as are those of the VHB4910 acrylic elastomer likewise actuated without prestrain (thick and thin dashed lines denote area and thickness strains, respectively).

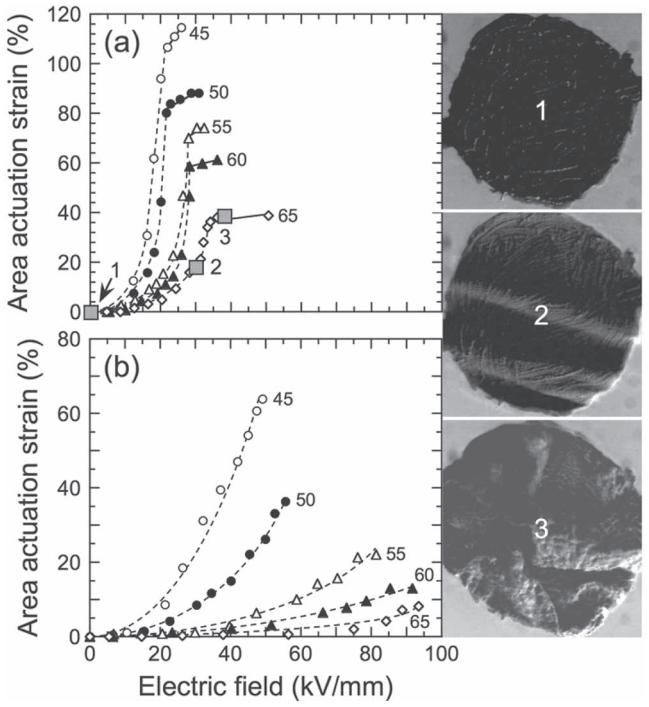

Figure 13. Area actuation strain displayed as a function of applied electric field for the a) MBM146 and b) MBM104 ATPEG series. Copolymer concentrations (in wt%) are labeled. Dashed lines serve as guides for the eye, while the solid lines are linear fits to the electromechanical (pull-in) instability regime. The images show the active (electrode) area in the MBM146-65 formulation in (a) at electric fields that are identified (grey squares) and numbered.

The in-plane actuation strain is presented as a function of the nominal electric field (normalized with respect to initial film thickness) in **Figure 13** for all the ATPEGs examined here. Although both ATPEG series display a similar and conventional response to the applied electric field, Figure 13a reveals an experimental phenomenon resulting from electromechanical stability[41] that has not been previously reported: buckling. As the applied electric field is increased, a film thins so that the actual electric field is higher than the nominal electric field. This increase in electric field promotes further nonuniform thinning of the DE, followed by eventual failure. Before failure, the constraints imposed by the relatively stiff boundary of the active area, coupled with electromechanical instability, promotes out-of-plane deformation, as evidenced by the development of specimen buckling. Images acquired from the MBM146-65 formulation at three electric fields are numbered in Figure 13a

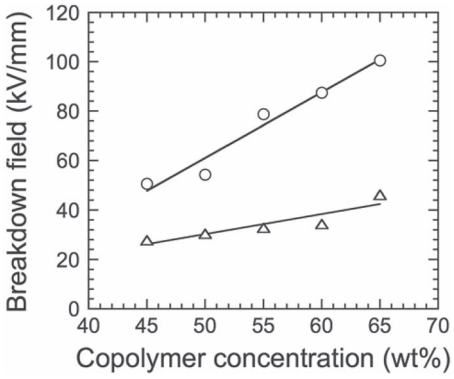

Figure 14. Maximum (breakdown) electric field displayed as a function of copolymer concentration for the MBM104 (○) and MBM146 (△) ATPEG series. The solid lines are linear regressions to the data and are provided as guides for the eye.

and show the formation of buckles, which is only observed in the case of the MBM146-based ATPEG series. We attribute this difference in electroactuation behavior to the lengths of the copolymer midblocks. Recall that the MBM104 copolymer possesses shorter midblocks that are extended upon microphase separation (before electroactuation). As the midblocks are stretched further at the onset of actuation, the film quickly stiffens to prevent the occurrence of instability.[41] Failure at higher electric fields is a consequence of dielectric breakdown, the second mode of soft dielectric material failure according to Zhao and Suo.[42] In the case of ATPEGs derived from the MBM146 copolymer, however, the midblocks are longer and can stretch more during actuation, thereby accommodating electromechanical instability. An implication of out-of-plane buckling is that the strain values (area and thickness) shown in Figure 12 are underestimated significantly.

The results displayed in Figure 13 permit direct comparison of the electric fields required for actuation. Maximum actuation (115% area strain) in the MBM146-45 system occurs at 26 kV/mm, whereas that in the MBM104-45 formulation (65% strain) requires a higher electric field (50 kV/mm). Under similar test conditions, the VHB4910 acrylic elastomer fails at 17–34 kV/mm after only ~7% actuation strain,[26] thus establishing the superior actuation performance of ATPEGs without mechanical prestrain. It is important to realize that the electric fields needed to actuate the ATPEGS in this work are generally lower than those required to actuate biaxially-prestrained DEs. While the precise reason for such improved actuation efficacy remains unclear, we contend that it is a consequence of the higher ε of the ATPEGs (due to the presence of DOP), in conjunction with the morphology-dependent mechanical properties of the materials. With regard to the latter consideration, a trend reported for DEs generated from SEBS-based TPEGs is that materials possessing the same (spherical) morphology exhibit overlapping trends in actuation strains and breakdown electric fields irrespective of copolymer molecular weight. In **Figure 14**, the dielectric breakdown field is consistently higher in the MBM104 series and increases linearly with increasing copolymer concentration in both ATPEG series. Recall that, with the exception of the MBM104-45 formulation, all the ATPEGs in the MBM104 series possess cylindrical morphologies. A bcc

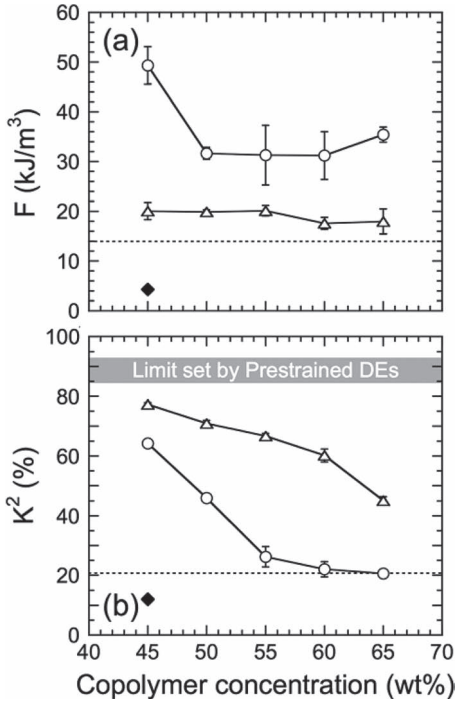

Figure 15. Dependence of a) energy density (F) and b) electromechanical coupling efficiency (K^2) on copolymer concentration for MBM104 (○) and MBM146 (△) ATPEGs subjected to electroactuation without mechanical prestrain. Error bars correspond to the standard error in the data. Corresponding results obtained under similar test conditions from the SEBS75-45 TPEG (◆) and VHB4910 acrylic elastomer (dashed line) are included for comparison. Solid lines serve to connect the data.

spherical morphology can therefore be reasonably anticipated at copolymer concentrations below 45 wt%. According to SAXS (cf. Figure 2 and 3), the spherical morphology does exist in the MBM146-45 system. Linear extrapolation of the two datasets displayed in Figure 14 provides the point of intersection at ~33 wt% copolymer, which corresponds to about 9 and 14 vol% M in the MBM146 and MBM104 series, respectively. At this concentration, a spherical morphology can be expected to form and, from the relationship established by Shankar et al.,[4] the actuation strains should be comparable. Difficulty associated with the preparation of such materials (which readily damage because they are excessively soft) has, however, thus far precluded experimental confirmation of this supposition.

Two additional electroactuation performance metrics introduced earlier in the Electroactuation Background and described in detail elsewhere[4,25] — the energy density (F) and electromechanical coupling efficiency (K^2) — are shown as functions of copolymer concentration in **Figure 15**a and Figure 15b, respectively. In Figure 15a, values of F determined from both ATPEG series are greater than those of the VHB4910 acrylic elastomer and SEBS75-45 TPEG. In addition, values of F calculated for the MBM146 series, while consistently lower than those from the MBM104 series, are nearly independent of copolymer concentration. This is not the case for K^2 shown in Figure 15b. Here, values of K^2 calculated for the MBM146 series are significantly and generally larger than those from the MBM104 series. The maximum values of K^2 from each series are 77 and 64%,

respectively, in marked contrast to 14% from the VHB4910 acrylic elastomer and 12% from the SEBS75-45 TPEG. It is important to recognize that the maximum efficiencies exhibited by the ATPEGs are higher than many DEs subjected to mechanical prestrain prior to electroactuation.[4] The current range of maximum efficiencies afforded by DEs (including those composed of VHB4910 or various TPEGs) are highlighted for completeness in Figure 15b. The results obtained from the MBM104-based ATPEG series display two intriguing features: (i) K^2 increases sharply with decreasing copolymer concentration, and (ii) K^2 levels off at the value of K^2 determined from the VHB4910 elastomer at high copolymer concentrations. Since F and K^2 are calculated from transverse strains and, as explained earlier, these strains are underestimated due to the onset of electromechanical instability, the values obtained for these metrics are also anticipated to be largely underestimated. Comparison of these performance metrics with those of mammalian skeletal muscle in Table 1 confirm that the ATPEGs investigated here generally possess comparable, if not superior, electroactuation characteristics relative to muscle and are therefore suitable, on this basis, for (micro)robotic applications. In addition, these materials constitute ideal candidates as functional materials for large-scale touchscreen devices (e.g., televisions and computer screens) in which DEs requiring mechanical prestrain could be irreparably problematic over time.

5. Conclusions

Thermoplastic elastomer gels composed of MBM triblock copolymers differing in molecular weight and composition and a low-volatility, B-selective solvent consist of M micelles (spherical or cylindrical) dispersed in a solvent-rich matrix. With the exception of one system (MBM104-45), all the MBM104 formulations examined here possess the hexagonally-packed cylindrical morphology, according to SAXS analysis. In marked contrast, the only morphology that could be conclusively assigned on the basis of SAXS data in the MBM146 series is spherical on a bcc lattice (for MBM146-45). Mechanical property analysis reveals that an increase in copolymer concentration promotes concurrent increases in the ultimate stress at failure and the tensile modulus due to a corresponding increase in the fraction of the glassy M endblocks. The Mullins effect, described as stress softening upon cyclic loading and unloading, is observed in the MBM104 ATPEG series, but not to the same extent in the MBM146 series. The existence of dispersed cylinders that microbuckle under stress are presumed to be responsible for this behavior. Due to its spherical morphology, however, the MBM146-45 system displays almost no evidence of this effect. This observation strongly suggests that, within the present ATPEG series, the dispersed elements comprising the copolymer nanostructure must be rigid (glassy) and irreversibly deform under an applied load for the Mullins effect to manifest. As expected, the mechanical properties of ATPEGs directly influence the electroactuation properties achieved, with stiffer materials exhibiting smaller actuation strains. Due to their relatively high dielectric constants, the present ATPEGs undergo actuation without any mechanical prestrain and at relatively low electric fields compared to other DEs. Measured actuation strains are sensitive to both copolymer nanostructure and tensile modulus. Electromechanical instability resulting in out-of-plane actuation appears as buckles and develops in the MBM146 series due most likely to the longer B midblock than in the MBM104 series. Cylindrical copolymer morphologies exhibit higher breakdown electric fields than spherical morphologies, thus confirming that the copolymer nanostructure directly influences the development of electromechanical properties. Maximum values of actuation (area) strain, energy density and electromechanical coupling efficiency — ~110%, ~50 kJ/m^3 and ~80%, respectively — match or exceed the electromechanical attributes of skeletal muscle (cf. Table 1), thereby making ATPEGs suitable for a wide variety of biomimetic applications, as well as advanced engineering and biomedical technologies.

Acknowledgements

This work was supported by the National Science Foundation. The authors thank Dr. Arjun Krishnan for valuable discussions.

Received: August 22, 2011
Published online: February 22, 2012

[1] a) *Thermoplastic Elastomers*, (Eds: G. Holden, H. R. Kricheldorf, R. P. Quirk), Hanser, Munich **2004**; b) D. J. George, *Handbook of Thermoplastic Elastomers*, PDL(Plastics Design Library)/William Andrew Pub., Norwich, NY **2007**.
[2] J. H. Laurer, J. F. Mulling, S. A. Khan, R. J. Spontak, R. Bukovnik, *J. Polym. Sci. B: Polym. Phys.* **1998**, *36*, 2379.
[3] a) N. Mischenko, K. Reynders, K. Mortensen, R. Scherrenberg, F. Fontaine, R. Graulus, H. Reynaers, *Macromolecules* **1994**, *27*, 2345; b) N. Mischenko, K. Reynders, M. H. J. Koch, K. Mortensen, J. S. Pedersen, F. Fontaine, R. Graulus, H. Reynaers, *Macromolecules* **1995**, *28*, 2054; c)K. Reynders, N. Mischenko, K. Mortensen, N. Overbergh, H. Reynaers, *Macromolecules* **1995**, *28*, 8699; d) H. Soenen, H. Berghmans, H. H. Winter, N. Overbergh, *Polymer* **1997**, *38*, 5653; e)H. Soenen, A. Liskova, K. Reynders, H. Berghmans, H. H. Winter, N. Overbergh, *Polymer* **1997**, *38*, 5661; f) J. R. Quintana, E. Diaz, I. Katime, *Polymer* **1998**, *39*, 3029; g) J. R. Quintana, M. D. Janez, E. Z. Hernaez, A. Garcia, I. Katime, *Macromolecules* **1998**, *31*, 6865; h)H. Watanabe, T. Sato, K. Osaki, *Macromolecules* **2000**, *33*, 2545; i)D. A. Vega, J. M. Sebastian, Y. L. Loo, R. A. Register, *J. Polym. Sci. B: Polym. Phys.* **2001**, *39*, 2183; j) J. R. Quintana, E. Hernaez, I. Katime, *Polymer* **2002**, *43*, 3217; k) K. Mortensen, E. Theunissen, R. Kleppinger, K. Almdal, H. Reynaers, *Macromolecules* **2002**, *35*, 7773; l) A. S. Krishnan, K. E. Roskov, R. J. Spontak, in *Advanced Nanomaterials*, (Eds: K. E. Geckeler, H. Nishide), Wiley-VCH, Weinheim, Germany **2010**, Ch. 26.
[4] a) R. Shankar, A. K. Krishnan, T. K. Ghosh, R. J. Spontak, *Macromolecules* **2008**, *41*, 6100; b) P. H. Vargantwar, S. M. Brelander, A. S. Krishnan, T. K. Ghosh, R. J. Spontak, *Appl. Phys. Lett.* **2011**, *99*, 242901.
[5] a) D. J. Kinning, E. L. Thomas, L. J. Fetters, *J. Chem. Phys.* **1989**, *90*, 5806; b) C. H. R. Kao, M. Olvera de la Cruz, *J. Chem. Phys.* **1990**, *93*, 8284.
[6] a) M. W. Hamersky, S. D. Smith, A. O. Gozen, R. J. Spontak, *Phys. Rev. Lett.* **2005**, *95*, 168306; b) M. E. Seitz, R. L. Rottsolk, K. R. Shull, *J. Polym. Sci. B: Polym. Phys.* **2010**, *48*, 1395.
[7] J. H. Laurer, S. A. Khan, R. J. Spontak, M. M. Satkowski, J. T. Grothaus, S. D. Smith, J. S. Lin, *Langmuir* **1999**, *15*, 7947.
[8] a) T. P. Lodge, B. Pudil, K. J. Hanley, *Macromolecules* **2002**, *35*, 4707; b) A. S. Krishnan, S. Seifert, B. Lee, S. A. Khan, R. J. Spontak, *Soft Matter* **2010**, *6*, 4331; c)T. L. Chantawansri, A. J. Duncan, J. Ilavsky, K. K. Stokes, M. C. Berg, R. A. Mrozek, J. L. Lenhart, F. L. Beyer, J. W. Andzelm, *J. Polym. Sci. B: Polym. Phys.* **2011**, *49*, 1479.

[9] A. Roos, C. Creton, *Macromolecules* **2005**, *38*, 7807.
[10] C. M. Flanigan, A. J. Crosby, K. R. Shull, *Macromolecules* **1999**, *32*, 7251.
[11] A. P. Sudarsan, J. Wang, V. M. Ugaz, *Anal. Chem.* **2005**, *77*, 5167.
[12] R. Shankar, T. K. Ghosh, R. J. Spontak, *Adv. Mater.* **2007**, *19*, 2218.
[13] N. Jullian, L. Rubatat, P. Gerard, J. Peyrelasse, C. Derail, *J. Rheol.* **2011**, *55*, 379.
[14] M. E. Seitz, W. R. Burghardt, K. T. Faber, K. R. Shull, *Macromolecules* **2007**, *40*, 1218.
[15] M. E. Seitz, D. Martina, T. Baumberger, V. R. Krishnan, C. Y. Hui, K. R. Shull, *Soft Matter* **2009**, *5*, 447.
[16] R. Pelrine, R. Kornbluh, Q. B. Pei, J. Joseph, *Science* **2000**, *287*, 836.
[17] J. D. W. Madden, N. A. Vandesteeg, P. A. Anquetil, P. G. A. Madden, A. Takshi, R. Z. Pytel, S. R. Lafontaine, P. A. Wieringa, I. W. Hunter, *IEEE J. Oceanic Eng.* **2004**, *29*, 706.
[18] T. Mirfakhrai, J. D. W. Madden, R. H. Baughman, *Mater. Today* **2007**, *10*, 30.
[19] R. Shankar, T. K. Ghosh, R. J. Spontak, *Soft Matter* **2007**, *3*, 1116.
[20] P. Brochu, Q. B. Pei, *Macromol. Rapid Commun.* **2010**, *31*, 10.
[21] E. Hornbogen, *Adv. Eng. Mater.* **2006**, *8*, 101.
[22] R. H. Baughman, C. X. Cui, A. A. Zakhidov, Z. Iqbal, J. N. Barisci, G. M. Spinks, G. G. Wallace, A. Mazzoldi, D. De Rossi, A. G. Rinzler, O. Jaschinski, S. Roth, M. Kertesz, *Science* **1999**, *284*, 1340.
[23] S. A. Wilson, R. P. J. Jourdain, Q. Zhang, R. A. Dorey, C. R. Bowen, M. Willander, Q. U. Wahab, M. Willander, M. A. H. Safaa, O. Nur, E. Quandt, C. Johansson, E. Pagounis, M. Kohl, J. Matovic, B. Samel, W. van der Wijngaart, E. W. H. Jager, D. Carlsson, Z. Djinovic, M. Wegener, C. Moldovan, R. Iosub, E. Abad, M. Wendlandt, C. Rusu, K. Persson, *Mater. Sci. Eng. R.* **2007**, *56*, 1.
[24] a) X. Q. Zhang, C. Lowe, M. Wissler, B. Jahne, G. Kovacs, *Adv. Eng. Mater.* **2005**, *7*, 361; b) F. Carpi, S. Bauer, D. De Rossi, *Science* **2010**, *330*, 1759.
[25] A. S. Krishnan, P. H. Vargantwar, T. K. Ghosh, R. J. Spontak, *J. Polym. Sci. B: Polym. Phys* . **2011**, *49*, 1569.
[26] R. Shankar, T. K. Ghosh, R. J. Spontak, *Macromol. Rapid Commun.* **2007**, *28*, 1142.
[27] a) M. Morton, J. E. Mcgrath, P. C. Juliano, *J. Polym. Sci. C: Polym. Symp.* **1969**, *26*, 99; b) L. S. Flosenzier, J. H. Rohlfing, A. M. Schwark, J. M. Torkelson, *Polym. Eng. Sci.* **1990**, *30*, 49.
[28] M. E. Seitz, W. R. Burghardt, K. R. Shull, *Macromolecules* **2009**, *42*, 9133.
[29] P. H. Vargantwar, R. Shankar, A. S. Krishnan, T. K. Ghosh, R. J. Spontak, *Soft Matter* **2011**, *7*, 1651.
[30] M. Mamodia, *Ph.D. Thesis - University of Massachusett*, Amherst, MA **2009**.
[31] A. S. Krishnan, J. H. Van Zanten, B. Lee, S. Seifert, R. J. Spontak, *Appl. Phys. Lett.* **2011**, *99*, 101908.
[32] M. W. Matsen, R. B. Thompson, *J. Chem. Phys.* **1999**, *111*, 7139.
[33] A. Dorfmann, R. W. Ogden, *Int. J. Solids Struct.* **2004**, *41*, 1855.
[34] P. A. Kakavas, *J. Appl. Polym. Sci.* **1996**, *59*, 251.
[35] J. Diani, B. Fayolle, P. Gilormini, *Eur. Polym. J.* **2009**, *45*, 601.
[36] M. Mamodia, A. Panday, S. P. Gido, A. J. Lesser, *Macromolecules* **2007**, *40*, 7320.
[37] A. D. Drozdov, *Int. J. Solids Struct.* **2009**, *46*, 3336.
[38] H. Jinnai, R. J. Spontak, T. Nishi, *Macromolecules* **2010**, *43*, 1675.
[39] A. F. M. Barton, *CRC Handbook of Polymer-liquid Interaction Parameters and Solubility Parameters*, CRC Press, Boca Raton **1990**.
[40] A. F. M. Barton, *CRC Handbook of Solubility Parameters and Other Cohesion Parameters*, CRC Press, Boca Raton **1983**.
[41] Z. G. Suo, *Acta Mech. Solida Sin.* **2010**, *23*, 549.
[42] X. H. Zhao, Z. G. Suo, *Phys. Rev. Lett.* **2010**, *104*, 178302.